Theory of action spectroscopy for single-molecule reactions induced by vibrational excitations with STM

T. Frederiksen,[1,2,*] M. Paulsson,[3,4] and H. Ueba[4]

[1]*Donostia International Physics Center (DIPC)–UPV/EHU, 20018 San Sebastián, Spain*

[2]*IKERBASQUE, Basque Foundation for Science, E-48011 Bilbao, Spain*

[3]*Department of Physics and Electrical Engineering, Linnaeus University, 391 82 Kalmar, Sweden*

[4]*Division of Nano and New Functional Materials Science, Graduate School of Science and Engineering, University of Toyama, Toyama 930-855, Japan*

(Received 15 November 2013; revised manuscript received 7 January 2014; published 23 January 2014)

A theory of action spectroscopy, i.e., a reaction rate or yield as a function of bias voltage, is presented for single-molecule reactions induced by the inelastic tunneling current with a scanning tunneling microscope. A formula for the reaction yield is derived using the adsorbate resonance model, which provides a versatile tool to analyze vibrationally mediated reactions of single adsorbates on conductive surfaces. This allows us to determine the energy quantum of the excited vibrational mode, the effective broadening of the vibrational density of states (as described by Gaussian or Lorentzian functions), and a prefactor characterizing the elementary process behind the reaction. The underlying approximations are critically discussed. We point out that observation of reaction yields at both bias voltage polarities can provide additional insight into the adsorbate density of states near the Fermi level. As an example, we apply the theory to the case of flip motion of a hydroxyl dimer $(OD)_2$ on Cu(110) which was experimentally observed by Kumagai *et al*. [Phys. Rev. B **79**, 035423 (2009)]. In combination with density functional theory calculations for the vibrational modes, the vibrational damping due to electron-hole pair generation, and the potential energy landscape for the flip motion, a detailed microscopic picture for the switching process is established. This picture reveals that the predominant mechanism is excitation of the OD stretch modes which couple anharmonically to the low-energy frustrated rotation mode.

DOI: 10.1103/PhysRevB.89.035427 PACS number(s): 68.37.Ef, 33.20.Tp, 68.35.Ja, 68.43.Pq

I. INTRODUCTION

Adsorbate motions on surfaces constitute the most fundamental step for many surface chemical reactions because it is the rate-limiting step for adsorbates to meet a reaction partner or to reach an active site before reaction takes place [1]. The observation of adsorbates motion and of formation/breaking of bonds on surfaces provides indispensable information about the microscopic mechanisms of surface chemical reactions [2]. Tunneling electrons from the tip of a scanning tunneling microscope (STM) can be used as an atomic-size source of electrons for electronic and vibrational excitations and to manipulate individual atoms and molecules in a controlled manner across a surface. Following the first observation of inelastic electron tunneling spectra (IETS) for a single acetylene molecule adsorbed on a Cu(100) surface with STM [3], Stipe *et al*. [4] reported that rotation of the acetylene molecule can be induced by vibrational energy transfer from the C-H stretch mode excited by tunneling electrons to the frustrated rotational mode of the molecule. The rotation rate $R(V)$ exhibits a threshold at the bias voltage corresponding to the excitation of the C-H stretch mode. Further, the slope $d\ln(R)/dV$ and the second derivative of the STM tunneling current d^2I/dV^2 both exhibit a peak at the same bias voltage $V \sim 358$ mV, thus demonstrating that the excitation of the C-H stretch mode is a trigger for rotation.

Since these pioneering works opened up the new avenues of STM-IETS and vibrationally mediated motions and reactions of single molecules on metal surfaces, a myriad of experimental and theoretical works have been accomplished [1,2]. It is well established that the observation of the reaction rate R as a function of tunneling current I and applied bias voltage V provides complementary and indispensable information about the microscopic elementary processes. Whereas $R(I)$ tells us how many inelastic tunneling electrons are required to induce a given single-molecule reaction (i.e., the reaction order), the quantity $R(V)$ reveals thresholds which may allow for assignment of the active vibrational modes responsible for inducing a given reaction.

Sainoo *et al*. [5] coined the study of vibrationally mediated motion yields, i.e., the yield $Y(V) \equiv eR(V)/I(V)$ that characterizes the probability per tunneling electron to actuate the motion, as "action spectroscopy" (AS) and emphasized that AS may reveal information about active vibrational modes of the adsorbate that are not visible in STM-IETS. In particular, they showed that for the configurational change of *cis*-2-butene on Pd(110), four vibrational modes could be detected in the AS, but only two of them in their STM-IETS. The underlying idea is that AS records all inelastic excitations responsible for the adsorbate motions and reactions, while IETS is only sensitive to inelastic scattering events that leave a correction in the current (and its higher derivatives). The latter is not guaranteed as, to lowest order in the electron-vibration coupling, the correction in the current is a competition between elastic and inelastic contributions which may cancel out [6–8]. Usually, $Y(V)$ has been measured to determine only the vibrational-mode energies that trigger a given reaction, and little attention has been paid to how much more that can be learned from a detailed analysis of AS.

*thomas_frederiksen@ehu.es

Ueba and Persson [9] demonstrated that AS, or more precisely the second derivative of the reaction rate $R(V)$ with respect to the bias voltage, in principle provides direct access to the vibrational density of states (DOS) $\rho_{\rm ph}(\omega)$ of the adsorbate. This led Motobayashi *et al.* [10] to propose a simple and empirical formula to reproduce $Y(V)$ over a wide range of V, resulting from integrating twice a Gaussian vibrational DOS. The spectral fitting of their formula to CO hopping and *cis*-2-butene configurational change on Pd(110) allowed a better determination of (i) the vibrational energy (compared to that estimated from a peak in $d\ln(R)/dV$), (ii) the reaction order, and (iii) the transition rate for CO hopping associated with anharmonic coupling between the modes excited by tunneling electrons and the reaction-coordinate (RC) mode.

Recently, we derived a general formula for $Y(V)$ in order to study H-atom relay reactions in a molecular chain of H_2O-OH-OH (D_2O-OD-OD) on Cu(110) [11]. This formula is quite general and can be applied to analyze also many other vibrationally mediated motions and reactions of single adsorbates on metal surfaces. One of us demonstrated this in a reproduction of $Y(V)$ for lateral hopping of a single CO molecule on Pd(110) [12,13]. From the extracted fitting parameters for the transition rate to excite the frustrated translation mode above the barrier, the anharmonic coupling between the C-O stretch mode excited by tunneling electron and the RC mode of the translation could be directly quantified for the first time.

In this work, we provide the detailed analytical procedures to obtain $Y(V)$ and discuss the various approximations involved. A key quantity, the vibrational generation rate $\Gamma_{\rm iet}(V)$ for vibrational excitations induced in the adsorbate by the tunneling current, is calculated directly from perturbation theory in the electron-vibration coupling (Fermi's golden rule). This simple approach for AS is in contrast to theories for IETS, where the need to quantify the inelastic corrections in the current generally demands more advanced formulations such as nonequilibrium Keldysh Green's functions (NEGF) [8,14]. We apply our formula to reproduce $Y(V)$ for the flip motion between the two stable configurations of a hydroxyl dimer $(OD)_2$ on Cu(110) [15–17]. The optimized adsorption geometry, the vibrational modes, and their relaxation through electron-hole pair excitations, as well as the potential landscape between the two different inclined configurations, are calculated by density functional theory (DFT) using VASP [18]. Conjoint with our previous work [19] based on INELASTICA [20] for the current-voltage characteristics, this work completes and deepens our theoretical understanding of the dynamics of the vibrationally induced flip motion of $(OD)_2$ on Cu(110).

The outline of the paper is the following. In Sec. II, a key quantity, the vibrational generation rate $\Gamma^{\nu}_{\rm iet}(V)$ for a normal mode vibration ν, is formulated using an adsorbate resonant model Hamiltonian. In doing so, a spectral generation rate $\Gamma^{\nu}_{\rm in}(\omega,V)$ corresponding to a vibrational excitation of energy $\hbar\omega_\nu$ is derived within perturbation theory in the electron-vibration interaction. The theoretical formulations are examined within several physical approximations, i.e., zero-temperature limit, linear expansion around emission threshold, and extended wide-band limit of the adsorbate density of states. We also examine how the shape of the vibrational density of states (δ, Gaussian, or Lorentzian functions) manifests itself in $\Gamma^{\nu}_{\rm iet}(V)$ near the threshold bias voltage for reaction. The main theoretical result is an analytic formula for the reaction yield $Y(V)$ which can be used to fit experiments on single-electron processes in order to gain insight into the involved vibrational modes and elementary reaction steps. In Sec. III, we apply the formula for $Y(V)$ to analyze the configurational switching of a hydroxyl dimer $(OD)_2$ on Cu(110) [15,17]. This analysis suggests that excitation of OD stretch modes is a trigger for switching through anharmonic coupling to the reaction coordinate. Finally, conclusions are presented in Sec. IV.

II. MODEL FOR VIBRATIONALLY ASSISTED SURFACE REACTIONS

A. Hamiltonian

To describe the typical STM setup, in which a tunnel current is passed through a single molecule or adatom adsorbed on a conductive surface, we consider the standard adsorbate resonance model Hamiltonian [21–24]

$$H_0 = \varepsilon_a|a\rangle\langle a| + \sum_s \varepsilon_s|s\rangle\langle s| + \sum_t \varepsilon_t|t\rangle\langle t| + \sum_s (V_{sa}|s\rangle\langle a| + \text{H.c.}) + \sum_t (V_{ta}|t\rangle\langle a| + \text{H.c.}), \quad (1)$$

written in terms of the one-particle electron states $|a\rangle$, $|s\rangle$, $|t\rangle$ of the adsorbate level, the substrate, and the tip, respectively, and their corresponding one-electron energies ε_a, ε_s, and ε_t. V_{sa} (V_{ta}) describes the hopping integrals between the substrate (tip) and the adsorbate level.

We further consider that a set of vibrational modes $\{\nu\}$ associated with the nuclear degrees of freedom of the adsorbate

$$H_{\rm vib} = \sum_\nu \hbar\Omega_\nu(b^\dagger_\nu b_\nu + 1/2) \quad (2)$$

couples to the adsorbate resonance via linear coupling terms

$$H' = \sum_\nu H'_\nu = \sum_\nu \chi_\nu(b^\dagger_\nu + b_\nu)|a\rangle\langle a|, \quad (3)$$

where χ_ν is the electron-vibration coupling matrix element for mode ν and b_ν ($b^\dagger_\nu$) the corresponding vibration annihilation (creation) operator. The system is therefore described by the following Hamiltonian:

$$H = H_0 + H_{\rm vib} + H'. \quad (4)$$

B. Reaction rate

At low temperatures, where molecular vibrations are almost completely frozen, the probability for a given adsorbate reaction or motion to occur is related to the efficiency for the tunneling electrons to excite the vibrational modes and thus to leave the adsorbate with sufficient energy to either overcome or tunnel through the potential energy barrier E_B associated with the reaction along the reaction coordinate (RC). Here, we limit ourselves to model reactions induced by single-electron tunneling events, which implies that adsorbate

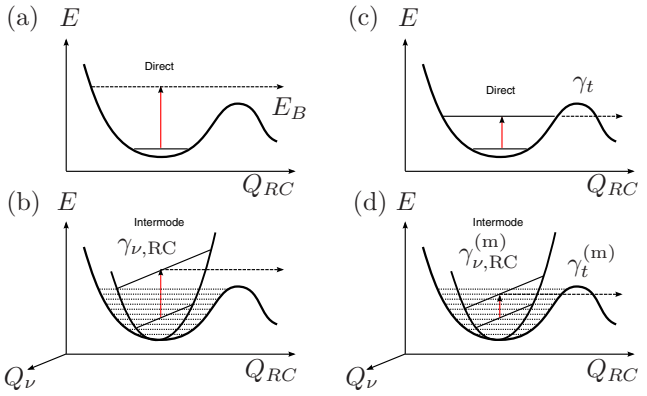

FIG. 1. (Color online) Schematic illustrations of four different elementary processes induced by single-electron inelastic tunneling events transferring a quantum of $\hbar\Omega$ (red arrows) to the adsorbate. The process may involve overbarrier (OB, $\hbar\Omega_\nu \geqslant E_B$, left column) or vibrationally assisted tunneling (VAT, $\hbar\Omega_\nu \leqslant E_B$, right column), and the accepting mode ν may be the RC mode itself (direct, top row) or involve intermode anharmonic coupling (bottom row) to the RC mode as characterized by the interconversion rate $\gamma_{\nu,\mathrm{RC}}$.

vibrational excitations are always damped before the next tunneling electron arrives.[1]

In this scenario, we can distinguish between four different elementary processes, sketched in Fig. 1, depending on whether it involves overbarrier (OB, $\hbar\Omega_\nu \geqslant E_B$) or vibrationally assisted tunneling (VAT, $\hbar\Omega_\nu \leqslant E_B$), and whether the accepting mode ν is the RC itself (direct, D) or involves intermode (IM) anharmonic coupling to the RC as characterized by the interconversion rate $\gamma_{\nu,\mathrm{RC}}$. We note that direct excitation of the RC [Fig. 1(a)] can not be quantified within the present theoretical framework because it involves direct coupling to the unbound (final) state.

For the common case of OB-IM elementary processes [Fig. 1(b)], the reaction rate $R^{\text{OB-IM}}$ is proportional to the (quasi)stationary population P_1^ν of the first excited state of the accepting mode and proportional to the interconversion rate $\gamma_{\nu,\mathrm{RC}}$ [24], i.e.,

$$R^{\text{OB-IM}}(V) = \gamma_{\nu,\mathrm{RC}} P_1^\nu. \tag{5}$$

The population P_1^ν is readily determined from the steady-state solution to the master equation (assuming $P_1^\nu \ll P_0^\nu \approx 1$)

$$\frac{dP_1^\nu}{dt} = -\left(\gamma_{\mathrm{eh}}^\nu + \gamma_{\nu,\mathrm{RC}}\right) P_1 + \Gamma_{\mathrm{IET}}^\nu(V) P_0^\nu = 0, \tag{6}$$

where $\Gamma_{\mathrm{IET}}^\nu(V)$ is the vibrational generation rate (the topic of the next subsection) due to the inelastic tunnel current that drives the oscillator from the ground state to the first excited state. In the above, we include only the electron-hole pair damping rate γ_{eh}^ν of mode ν, but other damping mechanisms can readily be added. The OB-IM reaction rate can thus be written as

$$R^{\text{OB-IM}}(V) = \frac{\gamma_{\nu,\mathrm{RC}}}{\gamma_{\mathrm{eh}}^\nu + \gamma_{\nu,\mathrm{RC}}} \Gamma_{\mathrm{IET}}^\nu(V) \simeq \frac{\gamma_{\nu,\mathrm{RC}}}{\gamma_{\mathrm{eh}}^\nu} \Gamma_{\mathrm{IET}}^\nu(V). \tag{7}$$

The reaction can also be induced by VAT γ_t by direct excitation of the RC mode itself [Fig. 1(c)]. In this case, we obtain

$$R^{\text{VAT-D}}(V) = \frac{\gamma_t}{\gamma_{\mathrm{eh}} + \gamma_t} \Gamma_{\mathrm{IET}}^{\mathrm{RC}}(V) \simeq \frac{\gamma_t}{\gamma_{\mathrm{eh}}} \Gamma_{\mathrm{IET}}^{\mathrm{RC}}(V), \tag{8}$$

which has been successfully applied to reproduce the experimental results of the hydrogen-bond exchange reaction within a single water dimer on Cu(110) [27,28].

The fourth possible single-electron process [Fig. 1(d)] corresponds to the case where the RC mode is first excited to the bundle of m levels below the barrier via decay of a mode ν excited by a tunneling electron via IM couplings $\gamma_{\nu,\mathrm{RC}}^{(\mathrm{m})}$, and then proceeds to escape by tunneling $\gamma_t^{(\mathrm{m})}$. In this case, the reaction rate is given by

$$R^{\text{VAT-IM}}(V) = \sum_m \frac{\gamma_{\nu,\mathrm{RC}}^{(\mathrm{m})} \gamma_t^{(\mathrm{m})}}{\left(\gamma_{\mathrm{eh}}^\nu + \gamma_{\nu,\mathrm{RC}}^{(\mathrm{m})}\right)\left(\gamma_{\mathrm{RC}}^{(\mathrm{m})} + \gamma_t^{(\mathrm{m})}\right)} \Gamma_{\mathrm{IET}}^\nu(V) \tag{9}$$

$$\simeq \sum_m \frac{\gamma_{\nu,\mathrm{RC}}^{(\mathrm{m})}}{\gamma_{\mathrm{eh}}^\nu} \frac{\gamma_t^{(\mathrm{m})}}{\gamma_{\mathrm{RC}}^{(\mathrm{m})}} \Gamma_{\mathrm{IET}}^\nu(V). \tag{10}$$

One factor represents the branching ratio of the ν mode decay via intermode coupling with respect to the total damping mechanisms of ν. A second factor represents the branching ratio of the tunneling from the level m with respect to the damping of the RC mode. Since the RC mode in general has a low energy associated with the nuclear motion, $\gamma_{\mathrm{RC}}^{(\mathrm{m})}$ contains both damping due to substrate phonons and generation of electron-hole pairs. To our knowledge there have been no experimental reports suggesting this VAT-IM scenario so far.

C. Vibrational generation rate

1. *Finite temperatures*

As is evident from the above, a key quantity in the theory of AS is the vibrational generation rate $\Gamma_{\mathrm{IET}}^\nu(V)$ associated with a characteristic vibrational (accepting) mode of the adsorbate being excited by the tunnel current. It can generally be expressed as [29]

$$\Gamma_{\mathrm{IET}}^\nu(V) = \int_0^\infty d\omega\, \rho_{\mathrm{ph}}^\nu(\omega) \Gamma_{\mathrm{in}}^\nu(\omega, V), \tag{11}$$

where $\rho_{\mathrm{ph}}^\nu(\omega)$ is the vibrational DOS and $\Gamma_{\mathrm{in}}^\nu(\omega, V)$ is the spectral generation rate for mode ν corresponding to an excitation of energy $\hbar\omega$ (phonon emission). Within Fermi's golden rule (FGR), the latter is given by

$$\Gamma_{\mathrm{in}}^\nu(\omega, V) = 2\frac{2\pi}{\hbar} \sum_{i,f} |\langle f; n+1 | H'_\nu | i; n \rangle|^2 \times n_a(\varepsilon_i, V)[1 - n_a(\varepsilon_f, V)]\, \delta_{\varepsilon_i, \varepsilon_f + \hbar\omega}, \tag{12}$$

where $|i; n\rangle$ ($|f; n+1\rangle$) characterizes the initial (final) electronic state with the harmonic oscillator in level n ($n+1$). A factor of 2 accounts for spin degeneracy. The Pauli exclusion principle is taken into account via the adsorbate level (energy-resolved) occupation probability $n_a(\varepsilon, V)$, which (under nonequilibrium conditions imposed by a sample voltage V)

[1]We note that this situation also includes combination band excitations [4,25] and coherent multiple excitation [26] in a single-electron tunneling process.

can be expressed as

$$n_a(\varepsilon, V) = \frac{n_F(\varepsilon + eV)\Gamma_s + n_F(\varepsilon)\Gamma_t}{\Gamma}, \tag{13}$$

where $\Gamma_{s/t}$ are the tunneling rates to substrate (s) and tip (t) electrodes [energy-independent quantities in the wide-band limit (WBL)], $\Gamma = \Gamma_s + \Gamma_t$ the total tunneling rate (lifetime broadening), and $n_F(\varepsilon) = 1/(e^{\beta(\varepsilon-\varepsilon_F)}+1)$ the Fermi-Dirac distribution function (Fermi energy ε_F, inverse temperature $\beta = k_B T$). With Eq. (3) as the perturbation we have

$$\Gamma^{\nu}_{\text{in}}(\omega, V) = 2\frac{2\pi}{\hbar}\chi_\nu^2 \sum_{i,f} |\langle n+1|b^\dagger + b|n\rangle|^2 |\langle f|a\rangle\langle a|i\rangle|^2 n_a(\varepsilon_i, V)[1 - n_a(\varepsilon_f, V)]\, \delta_{\varepsilon_i, \varepsilon_f + \hbar\omega} \tag{14}$$

$$= 2\frac{2\pi}{\hbar}\chi_\nu^2 [1 + n_B(\hbar\omega)] \int_{-\infty}^{\infty} d\varepsilon_i\ \rho_a(\varepsilon_i, V)\rho_a(\varepsilon_i - \hbar\omega, V) n_a(\varepsilon_i, V)[1 - n_a(\varepsilon_i - \hbar\omega, V)], \tag{15}$$

where $n_B(\hbar\omega) = 1/(e^{\beta\hbar\omega} - 1)$ is the Bose-Einstein distribution. The summations over initial and final states are replaced with integrals over the adsorbate DOS $\rho_a(\varepsilon, V)$ (per spin channel) defined via [21,22]

$$\rho_a(\varepsilon, V) = \sum_\alpha |\langle \alpha|a\rangle|^2 \delta_{\varepsilon, \varepsilon_\alpha}, \tag{16}$$

which in the WBL reads as

$$\rho_a(\varepsilon + eV) = \frac{1}{2\pi} \frac{\Gamma}{(\varepsilon + \eta eV - \varepsilon_a)^2 + (\Gamma/2)^2}. \tag{17}$$

Here, $\eta = \Gamma_s/\Gamma$ is a parameter that characterizes how the adsorbate level moves with voltage. In the following, we assume $\eta = 1$ corresponding to usual STM conditions where $\Gamma_s \gg \Gamma_t$. This implies that the adsorbate level is pinned to the substrate chemical potential, i.e., that an applied sample voltage V simply shifts the resonance position by eV with respect to the Fermi level ε_F. The full potential drop thus occurs between the adsorbate and STM tip. However, we note that for STM studies of adsorbate reactions on thin insulating films [30,31] it might be important (but straightforward) to take $\eta < 1$ explicitly into account.

2. Zero-temperature limit

To proceed further for $\Gamma_{\text{in}}(\omega, V)$ in Eq. (15) we apply successively a number of physical approximations. First, with the Lorentzian adsorbate DOS $\rho_a(\varepsilon)$ in Eq. (17), the spectral generation rate takes the following analytic expression in the zero-temperature limit ($k_B T \to 0$):

$$\Gamma^{\nu}_{\text{in},0}(\omega, V) = \frac{2\chi_\nu^2 \Gamma_s \Gamma_t}{\pi\hbar\Gamma(\Gamma^2 + (\hbar\omega)^2)} \times \begin{cases} \mathcal{I}(eV) - \mathcal{I}(\hbar\omega), & eV > \hbar\omega \\ \mathcal{I}(0) - \mathcal{I}(eV + \hbar\omega), & eV < -\hbar\omega \\ 0, & |eV| \leqslant \hbar\omega \end{cases} \tag{18}$$

where

$$\mathcal{I}(X) \equiv \mathcal{A}(X + \varepsilon_F - \varepsilon_a) + \mathcal{L}(X + \varepsilon_F - \varepsilon_a), \tag{19}$$

$$\mathcal{A}(X) \equiv \arctan\frac{2X}{\Gamma} + \arctan\frac{2(X - \hbar\omega)}{\Gamma}, \tag{20}$$

$$\mathcal{L}(X) \equiv \frac{\Gamma}{2\hbar\omega} \ln\frac{X^2 + (\Gamma/2)^2}{(X - \hbar\omega)^2 + (\Gamma/2)^2}. \tag{21}$$

The zero-temperature limit (denoted by subscript 0) is essentially always justified in STM manipulation experiments as the thermal energy is the smallest energy scale in the problem, e.g., at $T = 4.2$ K the thermal energy is $k_B T \approx 0.4$ meV, which is significantly smaller than typical vibrational excitations $\hbar\omega$, applied voltages eV, and lifetime broadenings Γ of the adsorbate resonance.

3. Linear expansion around emission onset

Second, as we are mostly interested in the behavior around the onset of vibrational emission, it is often a good approximation to perform a linear expansion of Eq. (18) around $eV = \pm\hbar\omega$. This can be written as

$$\Gamma^{\nu,\text{lin}}_{\text{in},0}(\omega, V) = \alpha(V)\gamma^{\nu}_{\text{eh}}(\omega)\frac{\Gamma_s\Gamma_t}{\Gamma^2}\frac{|eV| - \hbar\omega}{\hbar\omega}\theta(|eV| - \hbar\omega), \tag{22}$$

where θ is the Heaviside step function. We define $\gamma^{\nu}_{\text{eh}}(\omega) = 4\pi\omega\chi_\nu^2\rho_a^2(\varepsilon_F)$ as the "usual" electron-hole pair damping rate at ε_F and $\alpha(V) = \rho_a[\varepsilon_F + \text{sgn}(V)\hbar\omega]/\rho_a(\varepsilon_F)$ as an asymmetry factor taking into account variations in the adsorbate DOS on the energy scale of the vibrational energy. For an occupied resonance $\varepsilon_F - \varepsilon_a \geqslant \hbar\omega$, one has $\alpha(-V) > 1 > \alpha(+V)$, which according to Eq. (22) implies that the spectral generation rate in principle is larger for negative sample voltages than for positive.

4. Extended wide-band limit

Third, in the extended wide-band limit (EWBL), the adsorbate DOS is considered to be constant over the energy scale of the vibration energy, i.e., $\rho_a(\varepsilon \pm \hbar\omega) \approx \rho_a(\varepsilon)$ and therefore $\alpha(V) = 1$. The spectral generation rate thus takes the well-known form [24,29,32]

$$\Gamma^{\nu,\text{EWBL}}_{\text{in},0}(\omega, V) = \gamma^{\nu}_{\text{eh}}(\omega)\frac{\Gamma_s\Gamma_t}{\Gamma^2}\frac{|eV| - \hbar\omega}{\hbar\omega}\theta(|eV| - \hbar\omega). \tag{23}$$

We note that this result is readily recast to the form used in Ref. [32] by introducing the partial spectral functions defined as $A_{s(t)} = 2\pi\rho_a(\varepsilon_F)\Gamma_{s(t)}/\Gamma$.

5. Numerical comparison

Above we gave analytic expressions for the spectral generation rate $\Gamma_{\text{in}}(\omega, V)$ at various levels of approximations. Here, we compare them numerically and discuss the qualitative differences. Figure 2 shows the spectral generation rate for a specific set of parameters (see caption) for the adsorbate resonance model. The finite-temperature result [Eq. (15)] (thick red line) and the zero-temperature limit [Eq. (18)] (thick

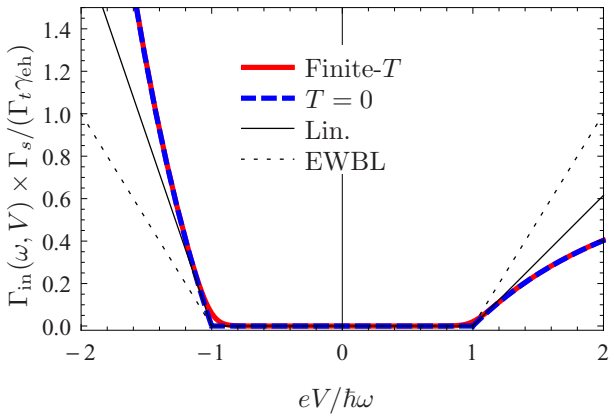

FIG. 2. (Color online) Generic illustration of the spectral generation rate $\Gamma_{\rm in}(\omega, V)$ at the various levels of approximations: the finite-temperature expression (15) (thick red line) and the zero-temperature expressions (18) (thick dashed blue line), (22) (linear expansion, thin black line), and (23) (EWBL, dashed-dotted black line). The model parameters are $\Gamma_s = 1000\Gamma_t = \varepsilon_F - \varepsilon_a = 90k_BT = 3\hbar\omega$, corresponding to a relatively sharp occupied electronic resonance at high temperatures (chosen to illustrate the differences between the various approximations).

dashed blue) coincide for voltages larger than the emission threshold $eV = \pm\hbar\omega$. Around the onset, finite temperature manifests itself in a smearing and finite emission probability below the threshold. Both expressions show a nonlinear dependence on V which originates from the energy dependence of the adsorbate resonance density of states $\rho_a(\varepsilon)$. For obvious reasons, the linear expansion Eq. (22) (thin black line) and the EWBL Eq. (23) (dashed-dotted black line) do not capture this nonlinearity, but the former maintains the asymmetry with respect to bias inversion [through the inclusion of the energy variation $\rho_a(\varepsilon_F - \hbar\omega) \neq \rho_a(\varepsilon_F + \hbar\omega)$].

For almost all practical purposes, the zero-temperature limit is valid to describe low-temperature STM-based experiments. The tiny effect of temperature observed in Fig. 2 is only visible because we chose a very high temperature compared with typical vibration frequencies of adsorbates at metal surfaces (we used $k_BT = \hbar\omega/30$ which implies that $T \sim 120$ K if $\hbar\omega = 300$ mV).

The more intricate approximations thus concern the handling of the energy dependence in $\rho_a(\varepsilon)$. To explore the accuracy of the linear expansion Eq. (22) [the EWBL Eq. (23)] in the full parameter space of the single electronic resonance, we take $(\Gamma^{\rm lin}_{\rm in,0} - \Gamma_{\rm in,0})/\Gamma_{\rm in,0}$ $[(\Gamma^{\rm EWBL}_{\rm in,0} - \Gamma_{\rm in,0})/\Gamma_{\rm in,0}]$ evaluated at $eV = 2\hbar\omega$ as a measure of the relative error. The results are shown in Fig. 3 for a fixed (weak) coupling to the tip, $\Gamma_t = \Gamma_s/1000$. The red (blue) areas correspond to overestimates (underestimates) of the spectral emission rate by ignoring the energy variation in the adsorbate DOS. The green lines mark the zero-error contours. From Fig. 3 one clearly sees that the linearization and EWBL approximations work well if $\Gamma_s \gg \hbar\omega$ (this condition will be satisfied for a chemisorbed molecule on metal surface with large level broadening Γ_s compared to the vibrational energy) or $\varepsilon_a \approx \varepsilon_F$ (on-resonance tunneling). The plots also reveal an apparent third condition where the error is zero (the green contour in the first quadrant). However, it is important to realize that this only corresponds to intersection of the voltage-dependent functions, i.e., for all other voltages $eV \neq 2\hbar\omega$ the spectral emission rates differ. By comparing Figs. 3(a) and 3(b), one observes the same qualitative features, but that the errors are somewhat larger in the EWBL. The particular set of parameters used in Fig. 2 is indicated in Fig. 3 by the black dot.

6. *Effect of the vibrational DOS*

As mentioned above [cf. Eq. (11)], we are going to take the vibrational DOS $\rho_{\rm ph}(\omega)$ explicitly into account for

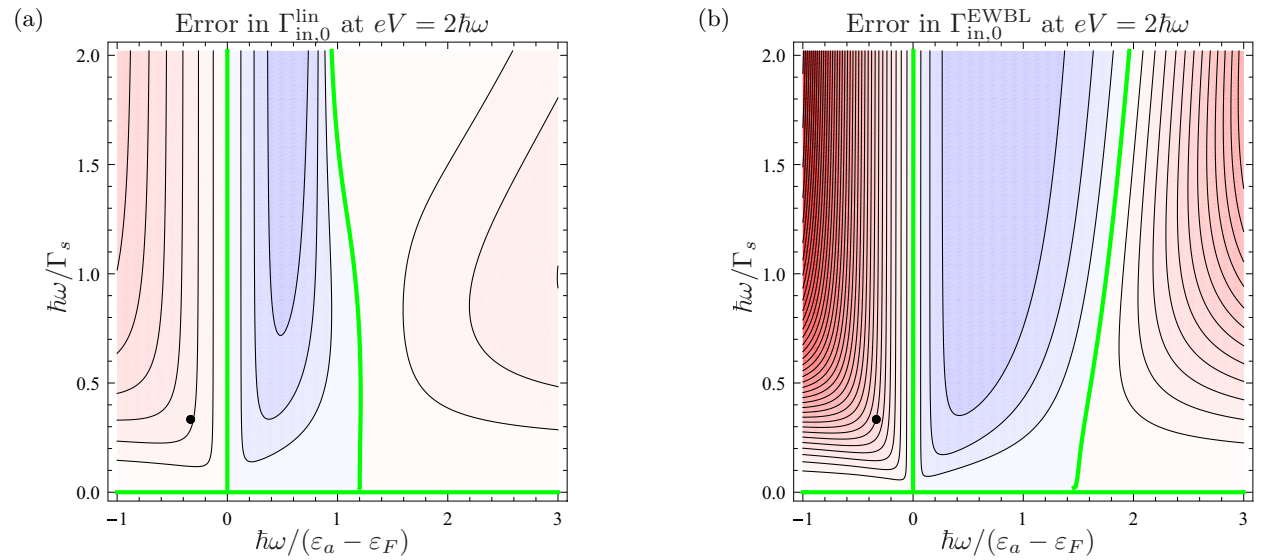

FIG. 3. (Color online) Relative errors in (a) $\Gamma^{\rm lin}_{\rm in,0}$ and (b) $\Gamma^{\rm EWBL}_{\rm in,0}$ (with respect to $\Gamma_{\rm in,0}$) evaluated at $eV = 2\hbar\omega$. Red (blue) areas correspond to overestimates (underestimates) of the spectral emission rate by ignoring the energy variation in the adsorbate DOS. The contour lines separate steps of 25%. The thick green lines mark the zero-error contours. The black dots indicate the specific set of parameters used in Fig. 2. We fix $\Gamma_t = \Gamma_s/1000$.

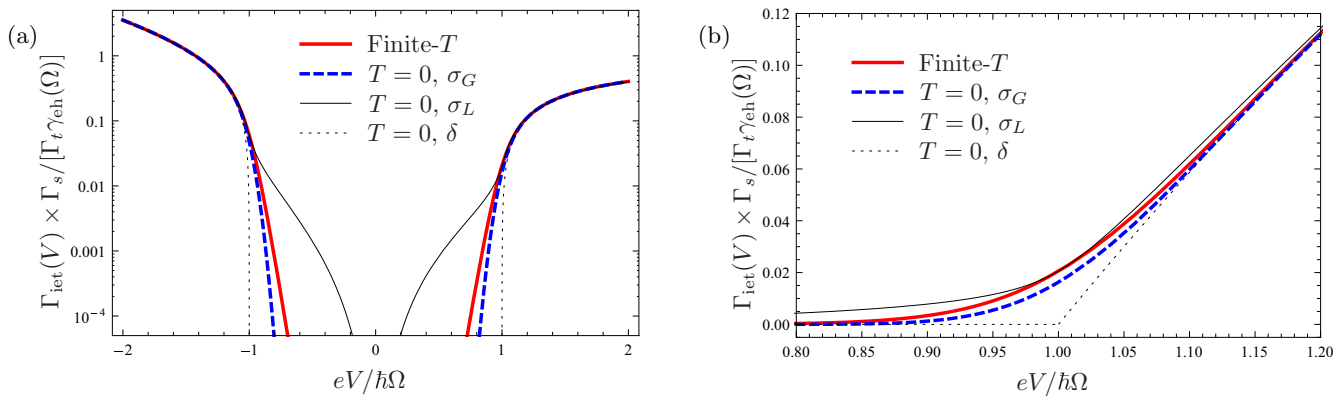

FIG. 4. (Color online) Generic illustration of the vibrational generation rate $\Gamma_{\rm IET}(V)$ on (a) a logarithmic scale for the whole bias range and (b) on a linear scale around the emission onset at positive sample voltage. The different curves correspond to the cases where the broadening is dominated by temperature (thick red line) or by a width in the vibrational DOS characterized by either a Gaussian ($\sigma_G = \hbar\Omega/15$, thick dashed blue line) or a Lorentzian ($\sigma_L = \hbar\Omega/15$, thin black line) distribution. For comparison, the result with a δ-DOS at zero temperature is also shown (dotted curve). The model parameters are $\Gamma_s = 1000\Gamma_t = \varepsilon_F - \varepsilon_a = 90k_BT = 3\hbar\Omega$.

the vibrational generation rate $\Gamma^{\nu}_{\rm iet}(V)$. We consider three different spectral forms as characterized by either a δ function or Gaussian/Lorentzian distributions centered around a characteristic vibrational energy $\hbar\Omega$, i.e.,

$$\rho^{\delta}_{\rm ph}(\omega) = \delta(\hbar\omega - \hbar\Omega) - \delta(\hbar\omega + \hbar\Omega), \tag{24}$$

$$\rho^{G}_{\rm ph}(\omega) = \frac{1}{\sigma_G\sqrt{2\pi}}\frac{1}{\mathrm{Erf}(\hbar\Omega/\sqrt{2}\sigma_G)}\left\{\exp\left(-\frac{(\hbar\omega-\hbar\Omega)^2}{2\sigma_G^2}\right) - \exp\left(-\frac{(\hbar\omega+\hbar\Omega)^2}{2\sigma_G^2}\right)\right\}, \tag{25}$$

$$\rho^{L}_{\rm ph}(\omega) = \frac{1}{4\arctan(2\hbar\Omega/\sigma_L)}\left\{\frac{\sigma_L}{(\hbar\omega-\hbar\Omega)^2+(\sigma_L/2)^2} - \frac{\sigma_L}{(\hbar\omega+\hbar\Omega)^2+(\sigma_L/2)^2}\right\}, \tag{26}$$

These DOS all satisfy the physical conditions $\rho_{\rm ph}(0) = 0$ and $\int_0^\infty \rho_{\rm ph}(\omega)d\omega = 1$.

Figure 4 explores the role of the different vibrational DOS spectra in $\Gamma_{\rm IET}(V)$. In general, we see that the vibrational generation rate is qualitatively different depending on the dominant source of broadening, namely, temperature or widths in the vibrational DOS. Away from the threshold for vibrational excitation $eV = \hbar\Omega$ temperature and Gaussian broadening display a rather similar voltage dependence (essentially exponential in the low-bias regime). However, as seen in Fig. 4(a), the Lorentzian line shape leaves a distinct shoulder on the logarithmic scale. From Fig. 4(b) it is clear that, even when parameters are chosen appropriately, each of the four cases also behave differently close to the emission threshold.

D. Reaction yield

Let us next turn our attention to the reaction yield $Y(V)$ defined by

$$Y(V) = \frac{R(V)}{I(V)/e} = \frac{K\Gamma_{\rm IET}(V)}{I(V)/e}, \tag{27}$$

where K is a proportionality factor (branching ratio) which depends on the kind of elementary process involved in the single-electron tunneling event [Fig. 1 and Eqs. (7)–(10)] and where $I(V)$ is the electrical current through the adsorbate level at an applied voltage V. The elastic current is given by

$$I(V) = \frac{2e}{\hbar}\frac{\Gamma_s\Gamma_t}{\Gamma}\int_{-\infty}^{\infty} d\varepsilon\, \rho_a(\varepsilon + eV)[n_F(\varepsilon) - n_F(\varepsilon + eV)], \tag{28}$$

where a factor 2 is included for spin.

1. Finite temperatures

When broadening of the reaction yield is dominated by temperature (i.e., not by vibrational broadening), one can evaluate Eq. (27) using Eq. (15) for the vibrational generation rate in combination with Eq. (28) for the current. A numerical example of this procedure is shown in Fig. 5 with red lines.

2. Vibrational broadened yields

Contrarily, when broadening of the reaction yield is dominated by effects well described by broadened vibrational spectra, one can resort to the zero-temperature limits for the spectral generation rate [Eq. (18)] as well as for the current:

$$I_0(V) = \frac{2e}{\pi\hbar}\frac{\Gamma_s\Gamma_t}{\Gamma}\left[\arctan\frac{2(eV-\varepsilon_a)}{\Gamma} + \arctan\frac{2\varepsilon_a}{\Gamma}\right]. \tag{29}$$

A numerical example of evaluating Eq. (27) with Eqs. (11), (18), (25), and (29) is shown in Fig. 5 with blue dashed lines.

3. Extended wide-band limit

Finally, useful analytic expression for the reaction yield can be stated in the EWBL approximation where it simply reads as

$$Y^{\rm EWBL}(V) = K_{\rm eff}\mathcal{F}(V, \rho_{\rm ph}), \tag{30}$$

where

$$K_{\rm eff} = \frac{\gamma_{\rm eh}(\Omega)}{2\Omega\Gamma\rho(\varepsilon_F)}K \tag{31}$$

is an effective (dimensionless) prefactor determined by the elementary process [K is the proportionality constant $R(V) = K\Gamma_{\rm iet}(V)$, see Eqs. (7)–(10)] and $\mathcal{F}$ is a voltage-dependent (dimensionless) function

$$\mathcal{F}(V,\rho_{\rm ph}) = \frac{1}{|eV|}\int_0^{|eV|} d\omega\,\rho_{\rm ph}(\omega)(|eV| - \hbar\omega). \tag{32}$$

To reach this expression we made use of the following approximation for the elastic current:

$$I_0^{\rm EWBL}(V) \approx \sigma_0 V, \tag{33}$$

where the zero-bias conductance σ_0 is simply

$$\sigma_0 = \frac{2e^2}{\hbar}\frac{\Gamma_s\Gamma_t}{\Gamma}\rho_a(\varepsilon_F). \tag{34}$$

The voltage-dependent function $\mathcal{F}$ takes the following analytic forms for each of the three considered vibrational DOS. With the δ function $\rho_{\rm ph}^{\delta}(\omega)$ it reads as

$$\mathcal{F}_\delta(V,\Omega) = \frac{|eV| - \hbar\Omega}{|eV|}\theta(|eV| - \hbar\Omega), \tag{35}$$

$$\lim_{eV\to\infty} F_\delta(V,\Omega) = 1, \tag{36}$$

with the Gaussian function $\rho_{\rm ph}^{G}(\omega)$

$$\mathcal{F}_G(V,\Omega,\sigma_G) = 1 + \frac{|eV| - \hbar\Omega}{|eV|}\mathcal{E}_G(|eV| - \hbar\Omega) - \frac{|eV| + \hbar\Omega}{|eV|}\mathcal{E}_G(|eV| + \hbar\Omega) + \frac{\rho_{\rm ph}(|eV|)\sigma_G^2}{|eV|}, \tag{37}$$

$$\mathcal{E}_G(X) = \frac{1}{2}\frac{\mathrm{Erf}(X/\sqrt{2}\sigma_G)}{\mathrm{Erf}(\Omega/\sqrt{2}\sigma_G)}, \tag{38}$$

$$\lim_{eV\to\infty} \mathcal{F}_G(V,\Omega,\sigma_G) = 1, \tag{39}$$

and finally with the Lorentzian function $\rho_{\rm ph}^{L}(\omega)$,

$$\mathcal{F}_L(V,\Omega,\sigma_L) = 1 + \mathcal{E}_L\left(\frac{|eV| - \hbar\Omega}{\sigma_L}\right) - \mathcal{E}_L\left(\frac{|eV| + \hbar\Omega}{\sigma_L}\right) + \left(i\frac{\sigma_L}{2|eV|} - \frac{\Omega}{|eV|}\right)\mathcal{E}_L\left(\frac{|eV|}{\sigma_L + i2\hbar\Omega}\right) - \left(i\frac{\sigma_L}{2|eV|} + \frac{\Omega}{|eV|}\right)\mathcal{E}_L\left(\frac{|eV|}{\sigma_L - i2\hbar\Omega}\right), \tag{40}$$

$$\mathcal{E}_L(X) = \frac{1}{2}\frac{\arctan(2X)}{\arctan(2\Omega/\sigma_G)}, \tag{41}$$

$$\lim_{eV\to\infty} \mathcal{F}_L(V,\Omega,\sigma_L) = 1. \tag{42}$$

The property $\mathcal{F} \to 1$ for $|eV| \to \infty$ implies that $Y^{\rm EWBL} \to K_{\rm eff}$, i.e., that the effective prefactor is essentially the saturation value of the reaction yield at high voltages.

Figure 5 shows numerical examples of evaluating Eq. (30) with Gaussian (thin black line) and Lorentzian (dashed black line) vibrational DOS. It also highlights a drawback of the EWBL approximation, namely, the loss of the fundamental asymmetry between the two bias polarities.

In most cases, the Gaussian distribution for the vibrational DOS provides the best agreement with experiments. This can be rationalized by considering that this distribution is most adequate to take into account *all broadening effects* encountered in practice (thermal, noise/instrumental, intrinsic lifetime broadening, and inhomogeneous broadening associated with random modulation of a vibrational energy) in a single parameter (the total width). Tikhodeev and Ueba [29] have shown that the broadening in the vibrational DOS due to finite-temperature effects is well represented by a Gaussian broadening, rather than the Lorentzian broadening associated with intrinsic vibrational relaxation due to electron-hole pair excitation.

When several vibrational modes ν are excited by the tunneling electrons, the yield should be expressed as the sum over contributions from each mode

$$Y^{\rm EWBL}(V) = \sum_\nu K_{\rm eff}^\nu \mathcal{F}\left(V,\rho_{\rm ph}^\nu\right). \tag{43}$$

This formula, in combination with a suitable model for the vibrational density of states, is our main result (based on EWBL) which takes a form that is readily applied to fit experimentally observed reaction yields due to single-electron processes.

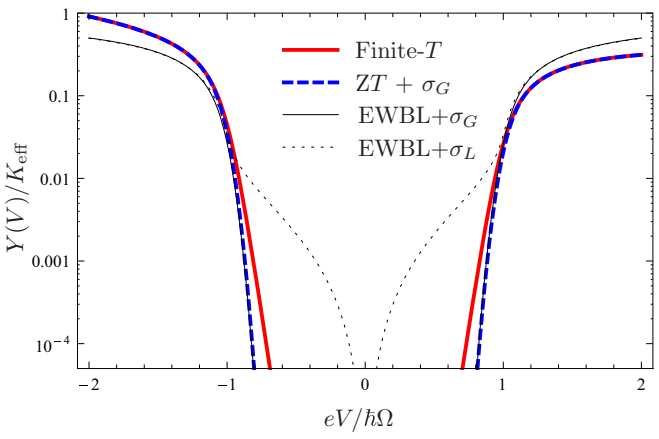

FIG. 5. (Color online) Generic illustration of the reaction yield $Y(V)$ in different limits. Two exact cases correspond to broadening dominated by temperature (thick red line) or by a Gaussian vibrational DOS (thick dashed blue curve). Two approximations are also shown: EWBL with a Gaussian (thin black line) and a Lorentzian (dotted black curve) vibrational density of states. The model parameters are $\Gamma_s = 1000\Gamma_t = \varepsilon_F - \varepsilon_a = 90k_BT = 45\sigma_G = 45\sigma_L = 3\hbar\Omega$.

4. On the bias polarity dependence

Our theory of STM-AS underlines the relevance of observing $Y(V)$ at both polarities as is usually done for STM-IETS in order to identify the vibrational fingerprints superimposed on a noisy background signal. Within the present adsorbate-induced resonance model, the vibrational modes are resonantly excited through a temporal occupation of the molecular orbitals (MO) by tunneling electrons, and excitation probabilities of vibrational modes depend on the population of the MOs at the corresponding energy. In this sense, STM-AS probes not only vibrational states but also electronic states near ε_F within a span of the vibrational energy of interest. Almost all STM-AS experiments reported so far concerned only positive bias voltages. However, we are aware of two interesting exceptions: (i) The yield reported for switching of an encapsulated Sc_3N cluster within a C_{80} fullerene cage [33] was essentially found to be independent on the bias polarity. This points toward a quite flat electronic DOS near ε_F (molecular resonances must be sufficiently far away in energy). In contrast, (ii) the yield observed for dissociation of an isolated dimethyl disulfide (DMDS) molecule $(CH_3S)_2$ on Cu(111) [34] was found to be orders of magnitude smaller for negative bias compared to that for positive bias. This observation was indeed explained by a large energy variation in the electronic DOS.

III. APPLICATION TO HYDROXYL DIMER SWITCHING

Recent low-temperature STM experiments [15,16] observed the configurational flip motion between the high (H) and low (L) conductance state of a hydroxyl dimer $(OD)_2$ on Cu(110), schematically shown in Fig. 6. The two hydroxyl groups, bonded to the adjacent bridge sites along (001), are oriented to take the optimal configuration for hydrogen bonding.

We previously reported a comprehensive theoretical analysis of the $(OD)_2$ on Cu(110) using DFT to determine the optimized geometry and vibration frequencies, the relative occupation of H and L conductance states as a function of the bias voltage, as well as the nonlinear current-voltage curves [19] using INELASTICA [20].

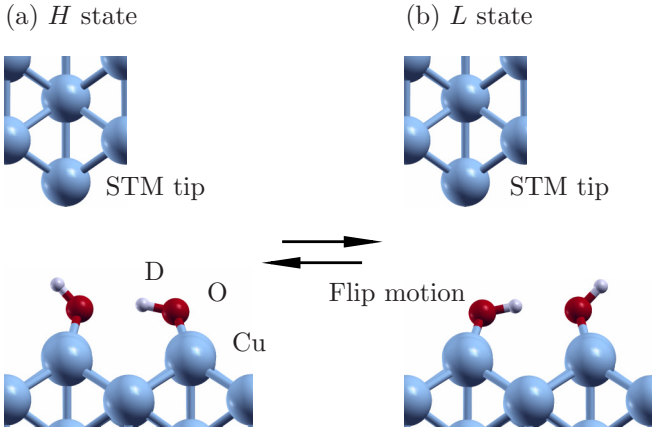

FIG. 6. (Color online) Schematic view of the high (H) and low (L) conductance states of a hydroxyl dimer $(OD)_2$ on Cu(110).

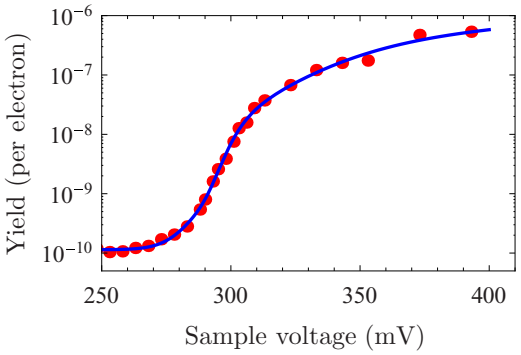

FIG. 7. (Color online) Yield of flip motion for a hydroxyl dimer $(OD)_2$ on Cu(110). The experimental data [17] (red circles) are well reproduced with a least-squares fit for the parameters $(\sigma^{\nu}_{\rm ph}, K^{\nu}_{\rm eff}, c)$ using Eq. (43) (blue line) with two vibrational modes characterized by the following parameters: $(\hbar\Omega^{(1)}, \sigma^{(1)}_{\rm ph}, K^{(1)}_{\rm eff}) = (299\ \text{meV}, 5\ \text{meV}, 5.5 \times 10^{-7})$, $(\hbar\Omega^{(2)}, \sigma^{(2)}_{\rm ph}, K^{(2)}_{\rm eff}) = (336\ \text{meV}, 20\ \text{meV}, 2.7 \times 10^{-6})$, and constant $c = 1.1 \times 10^{-10}$ (background due to low-energy modes).

Here, we focus on another aspect of the experiment, namely, the reaction yields [17] shown in Fig. 7 (red circles). As a demonstration of the theory developed in the previous sections, the figure also shows a least-squares fit for the parameters $(\sigma^{\nu}_{\rm ph}, K^{\nu}_{\rm eff}, c)$ to the experimental data using Eq. (43) with Gaussian DOS (blue line) assuming two active vibrational modes with energies 299 and 336 meV, respectively. The parameter c is a constant that represents a background due to low-energy modes. All parameters characterizing the model are given in the figure caption. The theory is able to reproduce the experimental data very well.

To gain insight into the fitting parameters and the underlying reaction mechanisms, we carried out DFT calculations with the projector augmented wave (PAW) method and a plane-wave basis as implemented in VASP [18]. The Cu(110) surface was modeled by a five-layer slab with a 4×3 periodicity (lattice constant $a = 3.64$ Å) and a vacuum region of ~11 Å between the slabs. We used a 515-eV energy cutoff, the Perdew-Burke-Ernzerhof [35] generalized gradient approximation (PBE-GGA) exchange-correlation functional, a 4×2 k mesh for Brillouin zone sampling, and the first-order Methfessel-Paxton scheme with 50-meV smearing for the Fermi surface. The adsorbate and two topmost Cu layers were relaxed until

TABLE I. Calculated vibrational-mode energies $\hbar\omega$ of a hydroxyl dimer $(OD)_2$ on Cu(110). The labelings ν, rot_{xy}, and rot_z refer to the stretch, parallel-to-surface rotation, and perpendicular-to-surface rotation, respectively.

Mode	$\hbar\omega$ (meV) This work	$\hbar\omega$ (meV) Ref. [19]
ν(OD)	336	327
ν(OD-O)	299	302
rot_{xy}(OD-O)	83	77
rot_z(OD-O)	80	77
rot_{xy}(OD)	58	52
rot_z(OD)	52	50

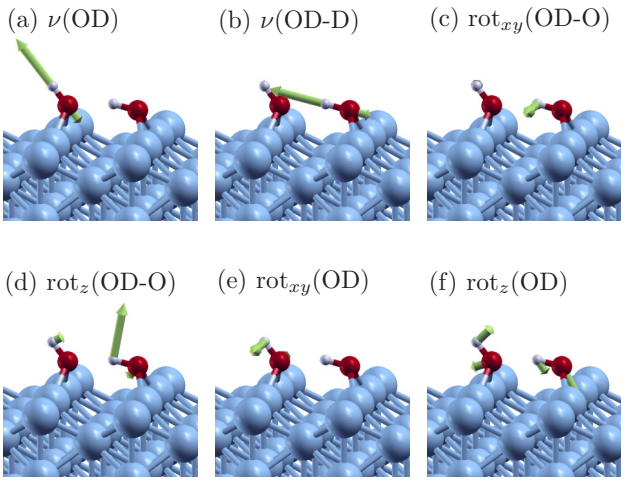

FIG. 8. (Color online) Illustration of the vibrational modes of a hydroxyl dimer $(OD)_2$ on Cu(110). The labelings ν, rot$_{xy}$, and rot$_z$ refer to the stretch, parallel-to-surface rotation, and perpendicular-to-surface rotation, respectively.

residual forces were smaller than 0.02 eV/Å. Vibrational modes and harmonic frequencies were calculated by finite differences with an amplitude of 0.02 Å in combination with a strict criterion for convergence of the electron density. Site-projected density of states (PDOS) was calculated using a Gaussian smearing of 0.25 eV and 8×8 k points (LORBIT = 11).

Computed harmonic mode energies $\hbar\omega$ are given in Table I for the six most energetic vibrations and the corresponding normal-mode vectors are shown in Fig. 8. Clearly, in the bias range of the reported reaction yield (Fig. 7), only the free ν(OD) and shared ν(OD-O) stretch modes are at play. In order to limit the number of fitting parameters, we therefore fixed the vibrational energies of the two modes to the calculated ones. The two stretch modes are thus the responsible accepting modes that couple to the reaction coordinate behind the switching process. Figure 9 shows the calculated two-dimensional contour potential map of $(OD)_2$ flip motion in terms of the D-atom coordinates along (001). A barrier between the two equivalent $(OD)_2$ configurations (initial and final states) is estimated to be about 300 meV, which is comparable to the energy of the shared ν(OD-O) mode and lower than the free ν(OD) mode.

Finally, Fig. 10 shows the PDOS onto the hydroxyl dimer $(OD)_2$ on Cu(110). An occupied molecular resonance is observed at about 1 eV below ε_F, which suggests that the parameters for a single-level model would be of the order $\Gamma_s \approx \varepsilon_F - \varepsilon_a \approx 1$ eV. The regime of these model parameters is indicated by a black dot in Fig. 3. Collecting the information above we can now proceed to estimate the intermode conversion rate $\gamma_{\nu,\mathrm{RC}}$ for a vibrationally assisted overbarrier process [Fig. 1(b)] via Eqs. (7) and (31) that simply combines to

$$K_{\mathrm{eff}} = \frac{1}{2\Omega}\frac{\gamma_{\nu,\mathrm{RC}}}{\Gamma\rho_a(\varepsilon_F)}. \tag{44}$$

Taking $\rho_a(\varepsilon_F) \approx 0.15$ eV/spin from Fig. 10, we find that $\gamma_{\nu(\mathrm{OD\text{-}O}),\mathrm{RC}} \approx 0.7 \times 10^8\ \mathrm{s}^{-1}$ and that $\gamma_{\nu(\mathrm{OD}),\mathrm{RC}} \approx 4 \times$

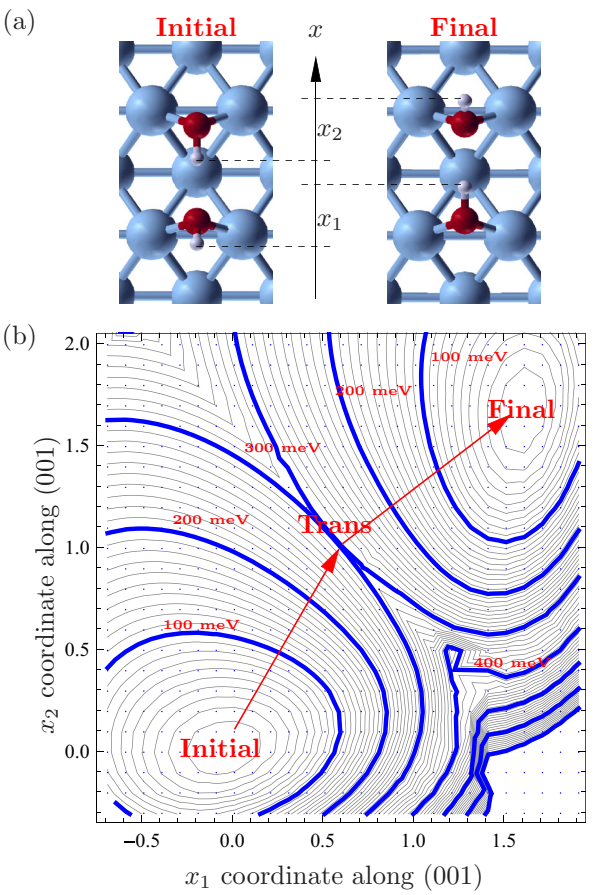

FIG. 9. (Color online) (a) Definition of D-atom coordinates (x_1, x_2) along (001). (b) Two-dimensional potential map of flip motion of a hydroxyl dimer $(OD)_2$ on Cu(110). For each set (x_1, x_2), the total energy was calculated relaxing all other degrees of freedom in the system (black dots). Contour lines (separated by 10 meV) were interpolated numerically from the regular grid of data points. The lowest-energy pathway from initial over transition to final state is schematically shown with red arrows.

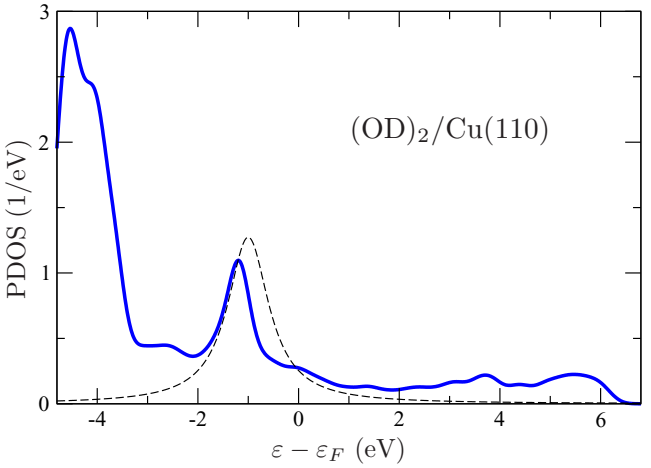

FIG. 10. (Color online) Projected density of states (PDOS) onto the hydroxyl dimer $(OD)_2$ on Cu(110) in the ground-state configuration (blue line). The occupied resonance suggests that parameters for a single-level model should be of the order $\Gamma_s \approx \varepsilon_F - \varepsilon_a \approx 1$ eV (dashed line).

10^8 s^{-1}. These transition rates indicate quite efficient intermode couplings compared to the electron-hole pair damping rates $\gamma_{eh} \approx 5 \times 10^{10}$ s^{-1} and 2.5×10^{11} s^{-1} reported in Ref. [19] for the shared and free OD stretch modes, respectively.

IV. CONCLUSIONS

We have presented a versatile formula of AS to analyze the reaction yield of single molecules induced by vibrational excitation with STM. In the present form, it applies to any single-electron processes (overbarrier, vibrationally assisted tunneling, or coherent multiple vibrational excitation [26]) but can readily be generalized to multielectron cases such as incoherent step-by-step vibrational ladder climbing [24,29]. Although the assignment of vibrational-mode energies can be made from conventional $\Delta \ln Y(V)/\Delta V$ plots, the present formula can be used even with a limited number of the experimental data points. The value of the obtained prefactor $K_{\rm eff}$ from experimental $Y(V)$ allows us to gain insights into the microscopic mechanisms of vibrationally mediated motions and reactions of single molecules on metal surfaces. As a demonstration we here applied the formula to the flip motion of a hydroxyl dimer $(OD)_2$ on Cu(110) in combination with vibrational modes and potential energy landscape obtained by DFT calculations. The analysis allowed us to estimate the intermode conversion rate from the shared and free OD stretch modes excited by tunneling electrons into the reaction coordinate.

Finally, the present theory also underlines the relevance of observing yields $Y(V)$ at both polarities as this would in principle provide information about variations in the adsorbate DOS near the Fermi level on the energy scale of the quantum associated with the accepting vibrational mode. In this way, STM-AS is a complementary experimental tool to explore not only dynamics of vibrationally mediated single-molecule reactions, but in principle also aspects of the electronic structure of the adsorbates.

ACKNOWLEDGMENTS

We are grateful to H. Okuyama and T. Kumagai for sharing their unpublished experimental results. T.F. acknowledges support from the Basque Departamento de Educacíon and the UPV/EHU (Grant No. IT-756-13), the Spanish Ministerio de Economy Competitividad (Grant No. FIS2010-19609-CO2-00), and the European Union Integrated Project PAMS. H.U. was supported by the Grant-in-Aid for Scientific Research (Grants No. S-21225001 and No. B-1834008) from Japan Society for the Promotion of Science (JSPS).

[1] H. Ueba, S. G. Tikhodeev, and B. N. J. Persson, *Inelastic Tunneling Current-Driven Motions of Single Adsorbates* (Pan Stanford Publishing, Singapore, 2010), Chap. 2, p. 373.
[2] W. Ho, J. Chem. Phys. **117**, 11033 (2002).
[3] B. C. Stipe, M. A. Rezaei, and W. Ho, Science **280**, 1732 (1998).
[4] B. C. Stipe, M. A. Rezaei, and W. Ho, Phys. Rev. Lett. **81**, 1263 (1998).
[5] Y. Sainoo, Y. Kim, T. Okawa, T. Komeda, H. Shigekawa, and M. Kawai, Phys. Rev. Lett. **95**, 246102 (2005).
[6] C. Caroli, D. Saint-James, R. Combescot, and P. Nozieres, J. Phys. C: Solid State Phys. **5**, 21 (1972).
[7] N. Lorente and M. Persson, Phys. Rev. Lett. **85**, 2997 (2000).
[8] H. Ueba, T. Mii, and S. G. Tikhodeev, Surf. Sci. **601**, 5220 (2007).
[9] H. Ueba and B. N. J. Persson, Phys. Rev. B **75**, 041403(R) (2007).
[10] K. Motobayashi, Y. Kim, H. Ueba, and M. Kawai, Phys. Rev. Lett. **105**, 076101 (2010).
[11] T. Kumagai, A. Shiotari, H. Okuyama, S. Hatta, T. Aruga, I. Hamada, T. Frederiksen, and H. Ueba, Nat. Mater. **11**, 167 (2012).
[12] T. Komeda, Y. Kim, M. Kawai, B. N. J. Persson, and H. Ueba, Science **295**, 2055 (2002).
[13] H. Ueba, Phys. Rev. B **86**, 035440 (2012).
[14] M. Paulsson, T. Frederiksen, H. Ueba, N. Lorente, and M. Brandbyge, Phys. Rev. Lett. **100**, 226604 (2008).
[15] T. Kumagai, M. Kaizu, H. Okuyama, S. Hatta, T. Aruga, I. Hamada, and Y. Morikawa, Phys. Rev. B **79**, 035423 (2009).
[16] H. Okuyama, A. Shiotari, T. Kumagai, S. Hatta, T. Aruga, Y. Ootsuka, M. Paulsson, and H. Ueba, Phys. Rev. B **85**, 205424 (2012).
[17] T. Kumagai and H. Okuyama (private communication).
[18] G. Kresse and J. Furthmüller, Phys. Rev. B **54**, 11169 (1996).
[19] Y. Ootsuka, T. Frederiksen, H. Ueba, and M. Paulsson, Phys. Rev. B **84**, 193403 (2011).
[20] T. Frederiksen, M. Paulsson, M. Brandbyge, and A.-P. Jauho, Phys. Rev. B **75**, 205413 (2007).
[21] D. M. Newns, Phys. Rev. **178**, 1123 (1969).
[22] B. N. J. Persson and M. Persson, Solid State Commun. **36**, 175 (1980).
[23] B. N. J. Persson and A. Baratoff, Phys. Rev. Lett. **59**, 339 (1987).
[24] S. Gao, M. Persson, and B. I. Lundqvist, Phys. Rev. B **55**, 4825 (1997).
[25] Y. E. Shchadilova, S. G. Tikhodeev, M. Paulsson, and H. Ueba, Phys. Rev. Lett. **111**, 186102 (2013).
[26] G. P. Salam, M. Persson, and R. E. Palmer, Phys. Rev. B **49**, 10655 (1994).
[27] T. Kumagai, M. Kaizu, S. Hatta, H. Okuyama, T. Aruga, I. Hamada, and Y. Morikawa, Phys. Rev. Lett. **100**, 166101 (2008).
[28] S. G. Tikhodeev and H. Ueba, Phys. Rev. Lett. **102**, 246101 (2009).
[29] S. G. Tikhodeev and H. Ueba, Phys. Rev. B **70**, 125414 (2004).
[30] P. Liljeroth, J. Repp, and G. Meyer, Science **317**, 1203 (2007).
[31] T. Sonnleitner, I. Swart, N. Pavlicek, A. Pöllmann, and J. Repp, Phys. Rev. Lett. **107**, 186103 (2011).
[32] M. Paulsson, T. Frederiksen, and M. Brandbyge, Phys. Rev. B **72**, 201101(R) (2005); **75**, 129901(E) (2007).
[33] T. Huang, J. Zhao, M. Feng, A. A. Popov, S. Yang, L. Dunsch, and H. Petek, Nano Lett. **11**, 5327 (2011).
[34] M. Ohara, Y. Kim, S. Yanagisawa, Y. Morikawa, and M. Kawai, Phys. Rev. Lett. **100**, 136104 (2008).
[35] J. P. Perdew, K. Burke, and M. Ernzerhof, Phys. Rev. Lett. **77**, 3865 (1996).